Rocky Worlds DDT: JWST Data Analysis Report for LHS 1140 b

Taylor J. Bell and Achrène Dyrek
JWST Data Analysis Team

October 20, 2026

1 Observation Overview

Under the RWDDT program, JWST-DDT-12498 Observation 1 obtained time-series imaging of LHS 1140 b using MIRI/F1500W with the BRIGHTSKY subarray, covering 8.75 hours with the goal of measuring the secondary eclipse of the planet. We measured both the centroid position and width of the target's point-spread function (PSF) during each integration. The telescope pointing remained fairly stable along the x and y axes throughout the observation, although there was some smooth variations in the y-centroid over time. The width of the PSF along both axes increased smoothly during the first $\sim$1 hour of the observation before settling to a fairly stable value (see Figure 1).

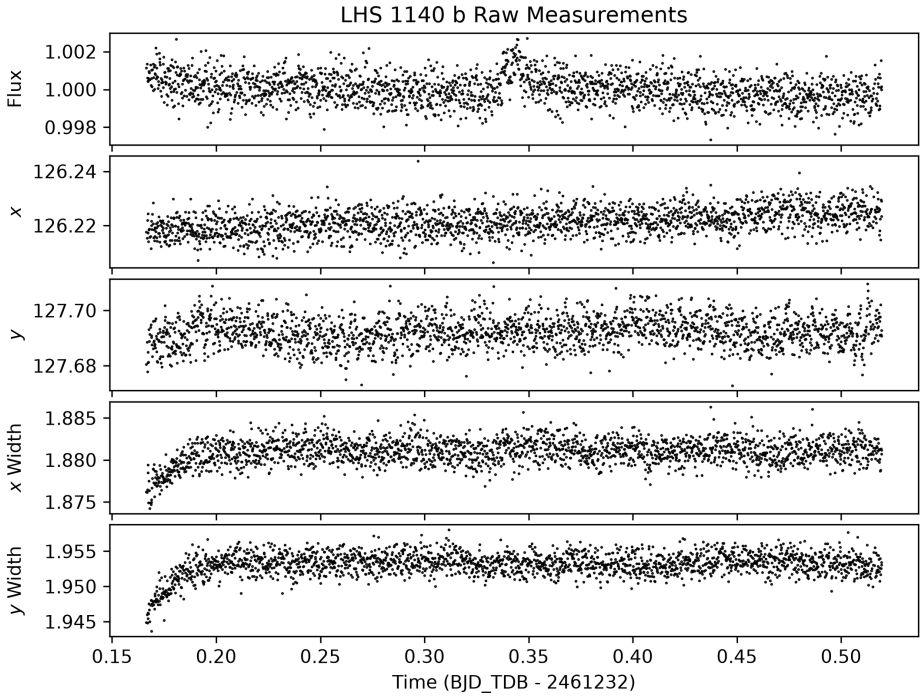

Figure 1: Measured flux and target centroid properties Time series of the relative changes in the normalized raw flux, centroid position (x, y), and PSF width (computed as the Gaussian standard deviation along the x and y axes), illustrating the initial settling behavior and overall stability of the telescope pointing and the PSF shape.

2 Data Reduction

This report presents results from one reduction and analyses performed by Bell and Dyrek. The analysis used the standard JWST pipeline (`jwst` v2.0.1 with CRDS context jwst_1535.pmap) for detector-level calibrations. Stage 1 processing included the following steps: `dq_init`, `emicorr`, `saturation`, `lastframe` (skipped), `reset`, `linearity`, `rscd` (with `rscd_group_skip1`=5 and `rscd_group_skip`=0), `dark_current` (skipped), `jump` (with the threshold at the default 4.0), and `ramp fitting`. In Stage 2 we ran `flat_field`, but we disabled the `photom` step as flux-calibrated data are not desired for time-series analyses.

Photometric extraction and light curve fitting were completed using Stages 3–5 of the `Eureka!` Python package (1.5.dev204+g0ead3741d). A time series was constructed for each pixel, and 4.5σ outliers (along with all `NaN` values) were replaced using bilinear interpolation over the nearest neighbors. Next, a center-of-mass centroid was calculated for each integration using the 'mgmc' method within `Eureka!`'s Stage 3. The position and width of the target's PSF along the x and y axes were measured in each integration using a 2D Gaussian fit (see Figure 1). These measurements were compiled into cotrending vectors that were subsequently used as independent variables in the systematics modeling.

Photometric light curves were extracted in Stage 3 of `Eureka!` using the `photutils` package with circular apertures and 'exact' edges, where pixels are weighted by the fraction of their area lying within the specified aperture. A range of aperture and background annulus radii were considered. Aperture radii ranged from 4–11 pixels, in 1-pixel steps. The inner radius of the background annulus varied from 14 to 26 pixels in 4-pixel steps, while the annulus width ranged from 10 to 30 pixels in 10-pixel steps. Photometric light curves were generated for each source aperture + background annulus pair. In Stage 4, both analysts chose to mask any integrations lying 4σ away from the rolling median using a boxcar filter with a width of 51 integrations.

After Stage 4 processing, the presence of a $\sim$1500 ppm bump in the middle of the lightcurve, around 2461232.34 $\mathrm{BJD_{TDB}}$, became evident. An analysis of the guide star telemetry, as well as the analysis of the MIRI centroid and PSF widths (see Figure 1), revealed no changes that coincided with this bump seen in the lightcurve. However, simultaneously with these JWST observations the Hubble Space Telescope (HST) observed LHS 1140 b using the Cosmic Origins Spectrograph (COS) under PID 18222, and these COS observations saw a similar bump at a similar time. We attribute this feature to a flare from the host star; perhaps the first stellar flare simultaneously observed in the UV and mid-IR. More details about the HST/COS observations will be presented in the separate HST data analysis report.

3 Light Curve Fitting

The dominant features of the white light curve are the detector settling ramp at the beginning of the observation and the stellar flare near the midpoint of the time series. To reduce the impact of the detector settling, the first 150 integrations were discarded prior to fitting. The light curve was modeled using an eclipse model multiplied by a flare

model and a systematic noise model. The full fitted model can be written as:

$$M(t) = E(t)\,F(t)\,S(t), \tag{1}$$

where $E(t)$ is the eclipse model generated with `batman`, $F(t)$ is the adopted flare model, and $S(t)$ describes the instrumental systematics. Our priors are summarized in Table 1.

Several approaches were investigated to account for the stellar flare during the light curve fit, including masking the flare-affected data, fitting only the data before the flare, or fitting the flare with either a symmetric or asymmetric Lorentzian profile. The asymmetric Lorentzian model is defined as

$$F(t) = \begin{cases} 1 + \dfrac{A_{\rm F}}{1 + \left(\dfrac{t - t_{\rm F}}{\gamma_{\rm F,LHS}}\right)^2}, & t \leq t_{\rm F}, \\ 1 + \dfrac{A_{\rm F}}{1 + \left(\dfrac{t - t_{\rm F}}{\gamma_{\rm F,RHS}}\right)^2}, & t > t_{\rm F}. \end{cases} \tag{2}$$

where A_F is the flare amplitude, t_F is the flare midpoint, and the γ_F terms the characteristic width of the event on either side of the flare midpoint. Meanwhile, the symmetric Lorentzian model simply sets $\gamma_{\rm F,LHS} \equiv \gamma_{\rm F,RHS}$. We found that the asymmetric Lorentzian model produced the highest Bayesian evidence compared the the symmetric Lorentzian model while also resulting in a cleaner RMS-binning plot (formerly known as an Allan variance plot). We note that the Lorentzian model is a parametric model of the flare and does not necessarily reflect the true, underlying astrophysical model.

Our systematic model is given by

$$S(t) = P(t)\,R(t)\,X\big(x(t)\big)\,Y\big(y(t)\big)\,SX\big(sx(t)\big)\,SY\big(sy(t)\big), \tag{3}$$

where

$$P(t) = c_0 + c_1(t - \bar{t}) \tag{4}$$

is a linear trend in time and

$$R(t) = 1 + r_0 \exp\left[-r_1(t - t_{\rm start})\right] \tag{5}$$

models the detector settling exponential ramp. The centroid position and PSF width decorrelation terms are each assumed to be linear, for example,

$$X(x) = 1 + c_x(x - \bar{x}), \tag{6}$$

where $(x(t), y(t))$ is the measured centroid position as a function of time, $(sx(t), sy(t))$ is the PSF width along the x- and y-axes as a function of time, $(\overline{x}, \overline{y})$ is the time-averaged centroid position, and $(\overline{sx}, \overline{sy})$ is the time-averaged PSF size.

All model parameters were sampled simultaneously using the `dynesty` dynamic nested sampling algorithm. We used an initial 105 live points with the 'rwalk' sampling algorithm and the 'multi' bounds and an initial $d\log\mathcal{L} < 0.01$ stopping criterion. Subsequent batches of 52 live points were then iteratively added with `pfrac` set to 0.5 (balancing the improvement in the precision of the posterior and evidence) until the default stopping criterion was achieved.

Table 1: The astrophysical and systematic model priors for the fits assuming a circular orbit. Fixed astrophysical parameters are shown without uncertainties and are taken from the juliet$_{circ}$ fit from CIT's orbit fitting efforts during observational scheduling. Gaussian priors are shown as $\mathcal{N}(\mu, \sigma)$ with mean μ and standard deviation σ, while Uniform priors are shown as $\mathcal{U}(l, u)$ with lower-limit l and upper-limit u.

Parameter	Prior	Posterior
P	24.7372456564 days	–
$t_{\rm sec}$	2461233.34496255 BMJD$_{\rm TDB}$	–
b	0.1416126966	–
a/R_*	95.2031220450	–
e	0	–
$R_*/R_\odot$ [†]	0.2159	–
$R_{\rm p}/R_*$	0.0743630409	–
$F_{\rm p}/F_*$	$\mathcal{N}(91, 200)$ ppm	157^{+52}_{-50} ppm
$A_{\rm F}$	$\mathcal{U}(0, 5000)$ ppm	1490 ± 110 ppm
$\gamma_{\rm F,LHS}$	$\mathcal{U}(0, 144)$ min	$1.30^{+1.2}_{-0.80}$ min
$\gamma_{\rm F,RHS}$	$\mathcal{U}(0, 144)$ min	$26.0^{+4.0}_{-3.5}$ min
$t_{\rm F}$	$\mathcal{N}(2461232.338, 0.05)$ BMJD$_{\rm TDB}$	$2461232.33799^{+0.00065}_{-0.00041}$ BMJD$_{\rm TDB}$
c_0	$\mathcal{N}(0.999, 0.01)$	$0.999749^{+0.000052}_{-0.000053}$
c_1	$\mathcal{N}(0.0, 0.1)$	$-0.00176^{+0.00019}_{-0.00020}$
r_0	$\mathcal{N}(0.00, 0.01)$	$0.00050^{+0.00022}_{-0.00020}$
r_1	$\mathcal{U}(3, 500)$	220^{+150}_{-110}
c_y	$\mathcal{N}(0.0, 0.5)$	$-0.0033^{+0.0029}_{-0.0029}$
c_x	$\mathcal{N}(0.0, 0.5)$	$0.0043^{+0.0035}_{-0.0034}$
c_{sy}	$\mathcal{N}(0.0, 0.5)$	0.012 ± 0.012
c_{sx}	$\mathcal{N}(0.0, 0.5)$	$0.046^{+0.012}_{-0.013}$
scatter_mult	$\mathcal{U}(0.8, 10)$	1.216 ± 0.018

[†]The stellar radius is used to account for the difference in light travel time throughout the planet's orbit.

3.1 Results & Discussion

The results of our fits are summarized in Table 1. Specifically, we find a eclipse depth posterior of 157^{+52}_{-50} ppm at the time predicted for a circular orbit. However, this fitted eclipse is coincident with a strong flare with a much larger amplitude of 1490 ± 110 ppm, and it is very possible that different reasonable treatments of the flare modeling could produce very different eclipse depth inferences. Further, because of the coincident stellar flare and the weak eclipse depth expected even for an airless scenario ($\lesssim$91 ppm; Espinoza et al., in prep.), we did not explore the possibility of a non-circular orbit with these analyses.

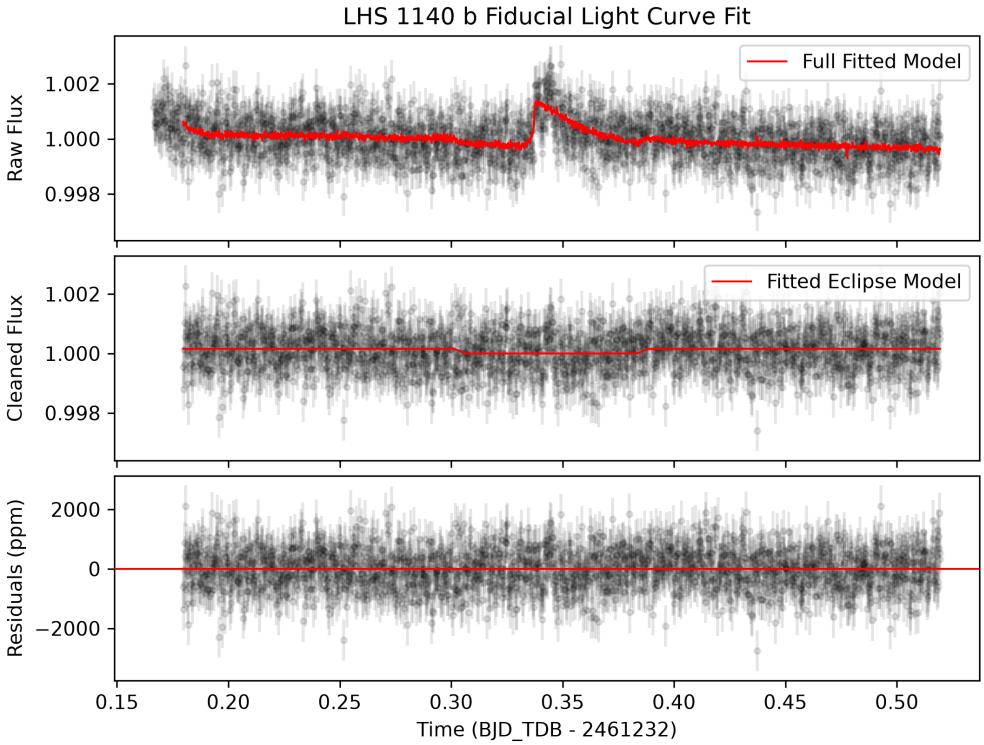

Figure 2: Fiducial light curve fit. *Top:* The raw, normalized flux measurements in black with the (systematic × astrophysical × Lorentzian model) over-plotted in red. The first 50 integrations were not included in the fit. *Middle:* The systematics-divided flux measurements are shown in black, with the fitted eclipse model shown in red. *Bottom:* The "data − model" residuals.

4 Calibrated Stellar Flux Measurement

Following the methodology of Gordon et al. (2025), we measured absolutely-calibrated stellar photometry using `calints` FITS files with a 5.69 px aperture and an 8.63–11.45 px background annulus, applying an aperture correction of 1.497. We added in quadrature the observational scatter with the $\sigma(\mathrm{CF}) = 0.48\%$ and $\sigma(\mathrm{repeat}) = 0.45\%$ terms from Gordon et al. (2025). As the light curve is impacted by a stellar flare occurring at the timing of the secondary eclipse, photometric calibration was performed using out-of-eclipse baseline data spanning 0.06 days on either side of the expected eclipse instead of using the in-eclipse baseline. This window excludes the part of the light curve impacted by the settling of the detector at the beginning of the observation, though there is a slight drift affecting the baseline over time. We obtained a calibrated stellar flux of 9.182 ± 0.060 mJy.

5 Discussion and Outlook

This report presents the analysis of the first RWDDT JWST eclipse observation of LHS 1140 b. No statistically significant eclipse signal was detected in these data. Instead, the dominant astrophysical feature is a ∼1500 ppm stellar flare occurring at the time the eclipse is expected. The contemporaneous HST/COS observations from the RWDDT in-

dependently detected a flare at the same time, providing strong evidence that the event is astrophysical in origin rather than instrumental. Several approaches were explored to account for the flare during the light curve analysis, with an asymmetric Lorentzian profile providing the preferred description of the data. The presence of such a large stellar event prevents a reliable measurement of the eclipse depth from this observation alone. Additional eclipse observations will therefore be required to disentangle stellar variability from the planetary signal and place meaningful constraints on the thermal emission of LHS 1140 b.